BIOMICROFLUIDICS 9, 064116 (2015)

# High efficiency vortex trapping of circulating tumor cells

Manjima Dhar,[1,2] Jessica Wong,[1] Armin Karimi,[1,2] James Che,[1,2] Corinne Renier,[3] Melissa Matsumoto,[1] Melanie Triboulet,[4] Edward B. Garon,[5] Jonathan W. Goldman,[5] Matthew B. Rettig,[6,7] Stefanie S. Jeffrey,[4] Rajan P. Kulkarni,[8] Elodie Sollier,[3,a)] and Dino Di Carlo[1,2,b)]

[1]*Department of Bioengineering, University of California Los Angeles, 420 Westwood Plaza, Los Angeles, California 90095, USA*
[2]*California NanoSystems Institute, 570 Westwood Plaza, Building 114, Los Angeles, California 90095, USA*
[3]*Vortex Biosciences, Inc., 1455 Adams Drive, Menlo Labs, Suite 2010, Menlo Park, California 94025, USA*
[4]*Department of Surgery, Stanford University School of Medicine, San Francisco, California 94305, USA*
[5]*Division of Hematology-Oncology, UCLA Medical Center, Los Angeles, California 90095, USA*
[6]*Department of Urology, UCLA Medical Center, Los Angeles, California 90095, USA*
[7]*Division of Hematology-Oncology, VA Greater Los Angeles Healthcare System, Los Angeles, California 90073, USA*
[8]*Division of Dermatology, UCLA Medical Center, Los Angeles, California 90095, USA*

(Received 20 October 2015; accepted 1 December 2015; published online 17 December 2015)

Circulating tumor cells (CTCs) are important biomarkers for monitoring tumor dynamics and efficacy of cancer therapy. Several technologies have been demonstrated to isolate CTCs with high efficiency but achieve a low purity from a large background of blood cells. We have previously shown the ability to enrich CTCs with high purity from large volumes of blood through selective capture in microvortices using the Vortex Chip. The device consists of a narrow channel followed by a series of expansion regions called reservoirs. Fast flow in the narrow entry channel gives rise to inertial forces, which direct larger cells into trapping vortices in the reservoirs where they remain circulating in orbits. By studying the entry and stability of particles following entry into reservoirs, we discover that channel cross sectional area plays an important role in controlling the size of trapped particles, not just the orbital trajectories. Using these design modifications, we demonstrate a new device that is able to capture a wider size range of CTCs from clinical samples, uncovering further heterogeneity. This simple biophysical method opens doors for a range of downstream interventions, including genetic analysis, cell culture, and ultimately personalized cancer therapy. © *2015 AIP Publishing LLC*. [http://dx.doi.org/10.1063/1.4937895]

## I. INTRODUCTION

Liquid biopsies of circulating tumor cells (CTCs) hold promise as a tool for studying primary and metastatic tumors. CTCs provide a minimally invasive way to track the evolution of genetic and molecular changes in tumors before, during, and after therapy to understand tumor evolution and select the most effective treatment strategies. However, the low quantity of CTCs in blood for some patients (~1–100 CTCs/ml)[1–3] introduces challenges in isolating them from a background of millions of leukocytes and billions of erythrocytes. Technologies that isolate CTCs must overcome the challenge of processing large volumes of blood quickly and

a)Email: elodie@vortexbiosciences.com.
b)Email: dicarlo@ucla.edu. Tel.: 310-983-3235.

 

concentrate these rare cells into manageable volumes for downstream analysis. Several cellular characteristics have been used to differentiate CTCs from leukocytes ,including surface protein expression, cell size, electrical properties, and cell deformability.[4] Surface markers are used to target either CTCs for positive selection or leukocytes for negative depletion.[3,5–8] In particular, the epithelial surface marker, epithelial cell adhesion molecule (EpCAM), and cytokeratin (CK) have been targeted in surface antigen-based CTC isolation and enumeration, respectively. Magnetic beads conjugated to antibodies targeting surface markers are used by the CellSearch semi-automated system, Adnagen and Isoflux.[5–7] Similar concepts have been applied to coat microfluidic device walls, micropillars, and nanotubes with anti-EpCAM antibodies.[9–11] Surface marker-based capture must be tuned to the cancer type, especially since not all cancer types and CTCs have significant EpCAM expression.[12,13] To further improve capture efficiency, cocktails of antibodies targeted towards a range of surface markers can be used. However, antigen-based capture often yields difficulty in integrating with downstream assays as cells remain attached to surfaces or beads and purity may be lower due to non-specific binding. Other technologies rely on physical properties of CTCs, including size-based filtration, acoustic wave deflection, resettable cell traps, and dielectrophoretic separation. Some of these technologies have limited throughput and/or require pre-processing steps, such as red blood cell-lysis or cell fixation, and/or often possess high level of contamination with leukocytes.[14–18]

More recently, size- and deformability-based isolation of CTCs have been demonstrated using continuous separation, which relies on inertial lift forces.[1,19,20] These technologies rely solely on microchannel geometry and do not require external electric or acoustic forces. In these devices, high Reynolds numbers coupled with various channel geometries lead to inertial forces that guide large and small cell populations such that each size focuses at different locations within the microchannel cross-section, where they can be selectively collected in separate outlets. Based on the channel geometry, smaller blood cells can focus near the channel side walls while larger CTCs focus closer to the center.[21] When combining with curving channels, cells focus faster at various lateral positions in the channel cross-section. Notably, these techniques maintain high efficiency (HE) capture and viability of cells. However, these devices still suffer from low purity and, because of the continuous flow extraction of CTCs from the diluted blood, often require additional concentration steps to be compatible with downstream assay volumes.

Previous work on trapping of larger cells in laminar microvortices has demonstrated the ability to quickly and passively enrich CTCs at high purity from a large volume of blood, and concentrate these cells in $<300\,\mu$l.[22–24] The Vortex Chip designed in this previous work efficiently captures cells larger than $\sim 15\,\mu$m in diameter, which is suitable to isolate many CTCs. However, this initial chip design may not trap some smaller CTCs. Many factors, including the geometry of the channels leading into the reservoirs, and the structure of the reservoirs themselves, could affect this size cut-off.

Here, we study the effects of channel geometry on tuning the efficiency, stability, and size cut-off for capture in the Vortex Chip—and we introduce the Vortex HE Chip. Vortex HE has higher efficiency capture for cells in a smaller size range ($>12\,\mu$m) than the Vortex Chip. This enables the capture of additional CTCs in patients with lung, prostate, and breast cancers. The ability to isolate a broader range of CTCs can better represent cellular diversity due to intra- and inter-tumoral heterogeneity. Capturing additional cells with rare mutations could aid in predicting response to treatment.[25–28] Importantly, although the cut-off in particle size is reduced, the Vortex HE mechanism maintains a highly pure sample, which benefits downstream molecular analysis.

## II. THEORETICAL BACKGROUND

When fluid with sufficient momentum travels through narrow entry channels that expand into large reservoirs, vortices are formed within the reservoirs. Cells that travel through the narrow entry channels migrate across fluid streamlines and into these predictable laminar microvortices (Fig. 1). Vortex formation and structure depends on the Reynolds number ($Re$) of the

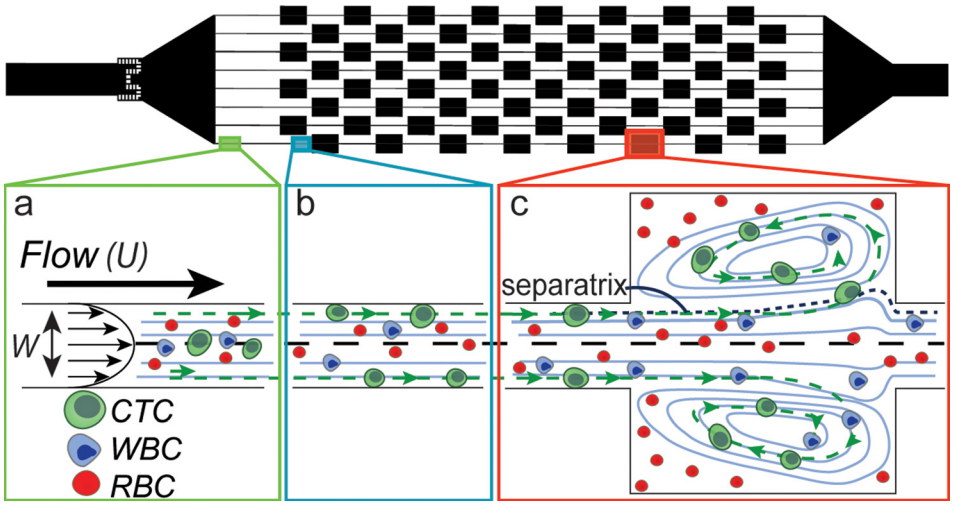


FIG. 1. Microfluidic device design. The Vortex HE device has 8 reservoirs in series and 8 in parallel. (a) Initially the red blood cells (RBCs), white blood cells (WBCs), and CTCs are distributed throughout the channel cross-section. (b) After traveling approximately 500 $\mu$m, the larger cells (CTCs) that experience higher inertial lift force migrate towards the channel walls. (c) The larger CTCs located near the wall experience enough lift force to enter the reservoir and remain stably trapped, while WBCs and RBCs either do not enter the reservoirs or do not remain trapped and return to the main flow.

entry channel. Here, $Re = \frac{\rho U D_h}{\mu}$, and $\rho$, $U$, and $\mu$ are the density, mean velocity, and dynamic viscosity of the fluid, respectively. $D_h$ is the hydraulic diameter of the channel, with $D_h = \frac{2WH}{W+H}$, where $W$ is the width and $H$ is the height of the channel. Two components critical for vortex trapping are a high number of particles entering into the vortices (*entry*) and the stable maintenance of trapped particles within the vortices (*stability*). First, particles must laterally migrate across the mainstream flow and cross the boundary of the vortex (the separatrix), due to fluid dynamic forces. These particles can then begin to circulate within the vortex. Second, these particles must be stable and maintain an orbit over several minutes within the vortex. Perturbations in the orbit of a particle could lead the particle to follow a trajectory that again crosses the separatrix and leaves the vortex trap to go back in the main flow.

Particle entry into reservoirs occurs due to shear-gradient lift force that acts down the parabolic profile developed in the entry channel.[24] The force scales as $F_L = \frac{f_L \rho U^2 a^3}{W}$, when $a/W$ is close to 1.[24] Here $f_L$ is the lift coefficient determined by the parabolic flow profile, $\rho$ is the density of the fluid, $U$ is the maximum fluid velocity, $a$ is the particle diameter, and $W$ is the width of the channel in the entry region prior to the reservoir. This force directs particles to cross the separatrix and enter the reservoir, because the parabolic profile developed in the entry channel is maintained for some distance downstream in the vortex region. Smaller particles do not experience enough shear-gradient lift force, and thus do not enter the reservoirs without other inter-particle collisions or hydrodynamic disturbances leading to entry. Equation for $F_L$ indicates that we can increase the shear-gradient lift force by decreasing the channel width ($W$), while maintaining a similar or larger flow velocity ($U$). This leads to a sharper parabolic flow profile and is expected to allow smaller particles to migrate across the separatrix as well and enter the reservoirs, where they may become stably trapped.

Once a particle enters into a reservoir, a variety of factors are expected to affect the particle stability. Inter-particle collisions or hydrodynamic interactions could disturb particles from stable orbiting streamlines within a vortex. Although hypothesized to affect trapping, no previous work has investigated the effect of background particle concentration on orbit stability and resultant effects on trapping efficiency. The volume capacity of the reservoir influences the density of the particles trapped and likelihood of inter-particle interactions. The parabolic velocity profile also decays downstream of the reservoir such that the shear gradient lift force that acts to restore trapped particles into stable orbits diminishes towards the end of the reservoir. This effect would become more pronounced when the reservoir is very long (Fig. S5).[29]

## III. EXPERIMENTAL SECTION

### A. Microfluidic device fabrication

Devices were made with the polymer polydimethylsiloxane (PDMS) using replica molding.[30] The mold structure was fabricated on a 4 in. silicon wafer (University Wafer Inc.) by photolithograpy. KMPR 1050 (Microchem) was spin coated with spin speed of 2900 rpm for 44 $\mu$m heights and 1700 rpm for 70 $\mu$m heights. Features were measured with a Dektak profilometer. The PDMS device was made with Sylgard 184 Elastomer (Dow Corning Corporation) with a cross-linker to polymer ratio of 1:10, and cured at 60 °C for 21 h. The devices were cut from the mold, and entry ports were punched using a 1.5 mm TiN coated biopsy needle (Syneo, LLC). The PDMS layer and a glass slide (VWR International, LLC) were $O_2$ plasma treated (Oxford Technics RIE) for 30 s, at 500 mTorr, 80 W power before being bonded together to enclose the microchannels.

### B. Study of particle entry mechanism into reservoirs

Polydisperse PDMS particles were made with silicone crosslinker and base polymer in a 1:10 ratio. 1 ml of PDMS was mixed with 50 ml of 0.01% Triton-X in deionized (DI) water, to stabilize PDMS droplets while curing and to form solid beads. The mixture was shaken in a vortexer for 5 min. The beads were cured at 60 °C for 24 h. PDMS particles less than 20 $\mu$m were separated using a 20 $\mu$m filter. Dilute polydisperse particles with a concentration of ~2500 particles per ml were infused into each device. Particle entry into reservoirs was quantified by analyzing high speed video of the particles as they entered or passed the reservoirs. The length of video analyzed was determined such that the same volume of fluid would be analyzed for each device, independent of flow rate used. Videos from six reservoirs were studied. A Phantom V2010 (Vision Research) high speed camera was used at a frame rate of 9000 frames/s. A semi-automated image processing algorithm developed in MATLAB was used to find the number and size of particles that either enter or pass by the reservoir. Entry analysis was performed for three devices with different channel widths and similar aspect ratios (W40 and H70, W24 and H44, and W18 and H44). The flow rates used for the entry study correspond to those which yielded the highest capture efficiency for each device.

### C. Stability analysis of particle orbits

We studied the stability of particles within their orbits by tracking the motion of one 20 $\mu$m polystyrene particle in the presence of background particles consisting of healthy whole blood, diluted to various ratios. Polystyrene beads were easily tracked, even among a high background of red blood cells (RBCs), due to the large difference in their refractive index from the surrounding cells. Diluted healthy whole blood was used to vary the level of perturbation in the system due to particle-particle interactions. A high speed camera (Phantom V2010) was used to capture videos at 3300 frames/s to characterize the orbit dynamics for one 20 $\mu$m bead trapped in a reservoir at a time. The plugin Mosaic Suite in ImageJ was used to track the particle trajectories.[31] A total of 250 trajectories were analyzed for five different reservoirs. The perturbation of the trajectories was defined by the transverse variance in the y direction of the trajectories. A cross section of the trajectories was taken as shown by the orange box in (Fig. 2(b)). The set of intersections of the trajectories through one x location (shown in Fig. 2(b) as a gray dashed lined) fit a Gaussian curve. The variance of the Gaussian is used to represent the variance of the trajectory and quantifies stability. The most stable trajectory would yield close to 0 variance, as shown in the graph of 0 RBCs in Fig. 2(b). The flow rates used were 2.62 ml/min for the devices with W24 and 4 ml/min for the devices with W40.

### D. COMSOL simulation

COMSOL Multiphysics 4.2a (COMSOL Inc.) was used to study variations in vortex formation in four different devices. Navier-Stokes equations for incompressible flow were used.

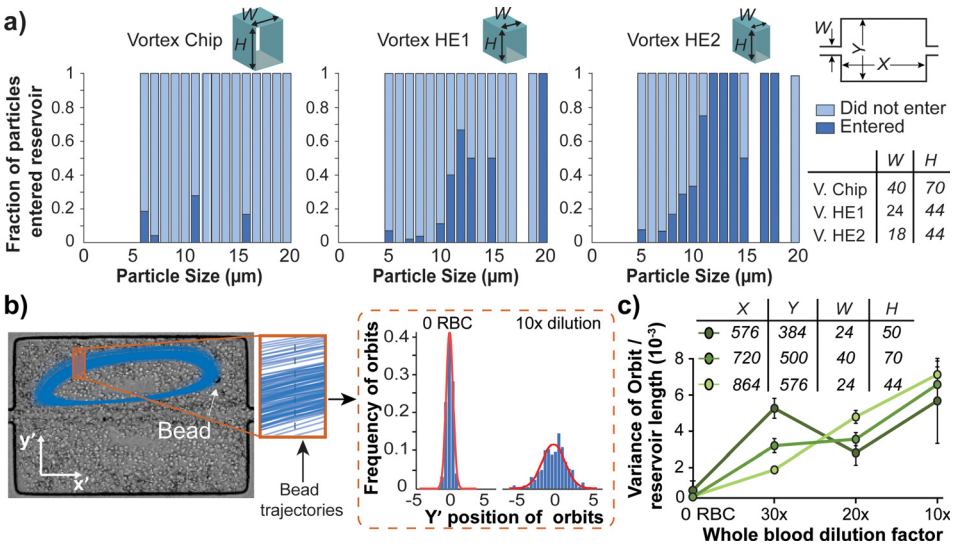


FIG. 2. Particle entry and orbit perturbation analysis. (a) Size distribution of particle entry depends on entry channel dimensions. The fraction of particles that enter the reservoir is the ratio between the number of particles of a particular size that entered the reservoir and the total number of particles of that size that were observed in the entry channel (dark blue bars). The light blue bars are the fraction of particles that did not enter the reservoirs. Blank spaces indicate no particles of that size was present. The size distribution and total number of particles entering into the system remained comparable between conditions (Fig. S3).[29] N = 6 reservoirs were used for each device. (b) Histograms of the points of intersection of a trajectory with one x position are shown. This is used to calculate a variance in intersection position, which quantifies the perturbation of the trajectory from a single consistent trajectory (most stable particles having a variance of 0). (c) Orbit variance analysis for 20 $\mu$m beads in PBS and 3 dilutions of blood, for N = 5 reservoirs.

No-slip boundary conditions were used at the walls, a symmetric boundary condition was used along the central horizontal axis of the device, and zero pressure boundary condition was used at the outlet (Fig. S5).[29] The inlet flow rates used for devices with 18 $\mu$m channel width and 44 $\mu$m height was 6.3 m/s, and flow rates for devices with 24 $\mu$m channel width and 44 $\mu$m height was 5.2 m/s.

### E. Cell line preparation

The non-small cell lung cancer (NSCLC) line A549 was used to model smaller cancer cells. These cell lines ranged from 11–27 $\mu$m in diameter when analyzed using brightfield imaging (Zeiss Axiovert, 10× objective) to characterize size. The prostate cancer cell line VCaP (diameter ranged from 12–35 $\mu$m) and breast cancer cell line MDA-MB-231 (diameter ranged from 12 to 29 $\mu$m) were also used to validate vortex HE devices. A549 cells were grown in RPMI-1640 media supplemented with 10% fetal bovine serum (FBS) and 1% penicillin-streptomycin-glutamine (P/S). MDA-MB-231 cells and VCaP cells were grown in DMEM, 10% FBS, and 1% P/S. Once the cells were semi confluent, they were lifted from their adherent layer using 0.25% Trypsin EDTA (Gibco) and 3 min incubation at 37 °C. The trypsin was neutralized with media and cells were spun down at 2500 rpm for 4 min. The trypsin and media were removed and the cells were suspended back in media before processing.

### F. Cell line spiking with PBS and blood

The vortex devices were operated using the procedure from Sollier *et al.*[22] For capture efficiency tests, the concentration of cells in suspension was determined using a hemocytometer, and appropriately diluted to 6000 cells per ml. Approximately 300 cells were spiked into 5 ml of PBS (Phosphate-Buffered Saline) and processed through the device. After collection in well plates, these cells were stained with a final concentration of 1 $\mu$g/ml Hoechst dye dissolved in water for 15 min, before imaging and enumeration. In order to mimic isolation of CTCs from blood, 300 cells were spiked into 0.5 or 1 ml of whole blood and diluted in PBS to 10 ml total

volume, for a 20× or 10× blood dilution, respectively. After processing, cells were fixed with 2% paraformaldehyde (Electron Microscopy Sciences) for 10 min, permeabilized with 0.4% v/v Triton X-100 dissolved in DI water (Research Products International Corp.) for 7 min, blocked with 5% goat serum diluted in PBS (Invitrogen) for 10 min and stained with final concentrations of 0.005 mg/ml DAPI (4′,6-diamidino-2-phenylindole, Molecular Probes), 0.05 mg/ml anti-CD45-PE (BD Biosciences, HI30), 0.025 mg/ml anti-CK-FITC (BD Biosciences, clone CAM5.2), 0.025 mg/ml anti-Pan-CK-FITC (MACS Miltenyi, clone CK3-6H5), and 0.025 mg/ml anti-CK -FITC (eBioscience, clone AE1/AE3) for enumeration. Clinical samples from lung cancer and breast cancer patients were also stained with 0.0002 mg/ml anti-Vimentin-AF647 (Abcam, clone V9) and 0.005 mg/ml anti-N-Cadherin-AF647 (Abcam, clone EPR1791-4) to evaluate epithelial to mesenchymal transition (EMT) status of CTCs. Prostate samples were also stained with 0.01 mg/ml anti-PSA (Dako, polyclonal) and a secondary antibody (Cell Signaling, Mouse anti-rabbit). Capture efficiency and capture purity were calculated as follows:

$$\text{Capture Efficiency} = \frac{\#\text{ of cancer cells collected}}{\#\text{ of cancer cells in control well}}, \tag{1}$$

$$\text{Purity} = \frac{\#\text{ of cancer cells}}{\#\text{ of cancer cells} + \#\text{ of WBCS}}. \tag{2}$$

### G. Cell viability and proliferation assay

Short term viability and longer term proliferation assays were conducted with A549 cells. Approximately 300 A549 cells were spiked into 5 ml of PBS, processed through Vortex HE1 and HE2 devices, and collected in well plates. As a control, A549 cells were directly transferred into the well plate with cell media, without being processed through the device. For viability assays, cells were stained with final concentrations of 5 $\mu$g/ml Calcein AM and 10 $\mu$g/ml of propidium iodide (PI-TRITC) for 15 min at room temperature after processing through devices. The cells were collected in the well plate, imaged, and enumerated. Live cells were identified as CalceinAM+/PI− while dead cells were CalceinAM±/PI+. Viability was defined by the ratio of live cells to total number of cells. For the cell proliferation assay, the cells were incubated at 37 °C with 5% $CO_2$ and monitored every day for 4 days.

### H. Patient studies

All blood samples were obtained with informed consent from patients and healthy donors, according to UCLA IRB#11-001798, UCLA IRB#11–001120, and Stanford IRB#5630. A total of 3 ml of blood was diluted 20× to 60 ml with PBS (Invitrogen) (60 ml final volume) and processed through the Vortex HE1 device at 2.6 ml/min. A separate 3 ml sample was also diluted 20× in PBS and was processed through the Vortex Chip at 4 ml/min. Age-matched healthy donors were processed in a similar manner, with 1 male control for prostate, 1 female control for breast, and an additional control for lung (Supplementary Table 1).[29]

Cells collected from the blood samples were stained using the same protocols as cell lines spiked in blood. After staining, each well was imaged using a Photometrics CoolSNAP HQ2 CCD camera mounted on an Axio Observer Z1 microscope (Zeiss), with an ASI motorized stage operated with Zen software. CTCs collected from lung and breast samples were classified as DAPI+/CK+/CD45− or DAPI+/CK−/CD45− with a nucleus larger than 9 $\mu$m and a high nuclear to cytoplasm ratio.[32] The 9 $\mu$m size cut off metric is based on a large nuclear size classified as malignant in tumor cytomorphological analysis. CTCs from prostate samples were classified according to the same criterion in addition to being DAPI+/CK±/CD45−/PSA+. Detailed enumeration criteria are shown in Fig. S8.[29] The samples were enumerated manually by two reviewers. After the first reviewer marked the CTCs and white blood cells (WBCs), the second reviewer verified each marking.

## IV. RESULTS AND DISCUSSION

### A. Decoupling particle entry in the vortices versus stability

In agreement with predictions from the equation for $F_L$, we found that devices with smaller channel width and higher maximum velocity improved particle migration into the reservoirs. When maintaining a constant Reynolds number of 160 between devices, the Vortex HE2 design with channel width of 18 $\mu$m and height of 44 $\mu$m had the highest fraction of particles enter reservoirs, compared with Vortex HE1 with a channel width 24 $\mu$m and height of 44 $\mu$m (Fig. 2(a)). The entry of particles in the Vortex Chip device was analyzed as well for reference (width 40 $\mu$m and height of 70 $\mu$m). Vortex Chip was operated at Re 150, which is the optimal Re at which the most particles can be trapped in this device.[22] In a channel with smaller cross sectional area, the maximum velocity within the channel is much higher for a constant Reynolds number. The smaller channel width also contributes to a sharper parabolic flow profile. These factors lead to a higher shear-gradient lift force experienced by all particles. As Fig. 2(a) shows, 3 times more fraction of the particles in the size range of 8–11 $\mu$m can enter the HE1 and 7 times more can enter HE2 devices than Vortex Chip. Our observations indicate that as $a/W$ increases, entry in reservoir increases as well, which is consistent with previous reports that indicated increased entry as $a/W$ approaches 1.[24]

The results from particle entry suggest that the particle entry mechanism is mainly dominated by the entry channel dimensions, but is independent of reservoir size. The fraction of particles that enter devices with channel width 18 $\mu$m and 24 $\mu$m but with smaller reservoirs remained similar as with larger reservoirs (Fig. S4).[29]

Once particles enter the reservoir, they must remain stably trapped in their orbit to be captured. We found that the stability of particle orbits increases with decreasing background levels of blood cells. We characterize the perturbation of a bead from its stable orbit by the variance of a Gaussian fit to a defined portion of its trajectory (Fig. 2(b)). Variance for 20 $\mu$m polystyrene bead orbits with a background of $2.5 \times 10^5$ RBCs (corresponding to 20× dilution) was half of the background level of $5 \times 10^5$ RBCs (corresponding to 10× dilution). Fig. 2(c) indicates that orbit stability is independent of reservoir dimensions. The dilution of blood seems to be the main factor influencing stability. Lower orbit perturbations are expected to increase stability of trapping, and reduce the likelihood of particles to again cross the separatrix and enter the main flow once they have entered the vortex trap. Previous studies have demonstrated that the capture efficiency of cells spiked in blood increases with the dilution of blood,[22] which we now show is partly due to changes in the orbit variance with increasing background cell levels. Based on these results, further studies with CTC isolation in this work were performed with 20× diluted blood.

### B. Device validation with cell lines

The results from particle entry experiments indicate that a reduced channel width, when Reynolds number is kept constant, may enhance capture efficiency of cells. We tested our hypothesis with A549 cell lines spiked in PBS, which have reduced capture efficiency with Vortex Chip due to their smaller size.[33] The capture efficiencies of two devices with constant height of 44 $\mu$m, constant Re of 160, and differing widths of 18 $\mu$m (HE2) and 24 $\mu$m (HE1) show that the device with the smallest width has the highest capture efficiency of 69% (Fig. 3(a)), a 7 fold increase over Vortex Chip. The Re of 160 is used because it has the highest capture out of the range tested (Fig. S2).[29] Increased efficiency is due to capture of more cells and cells of smaller sizes. Although the average diameters of cells caught by HE devices and Vortex Chip remain constant at approximately 18 $\mu$m, the minimum diameter of cells caught by HE1 is 11 $\mu$m and HE2 is 13 $\mu$m while Vortex Chip is higher at 15 $\mu$m. Other device parameter variations, such as changing the height to 50 $\mu$m while maintaining the width at 18 $\mu$m, do not improve capture significantly (Fig. S2).[29]

The results from A549 capture experiments are consistent with the expectations from equation for $F_L$. When the width of the entry channel is decreased from the original 40 $\mu$m to

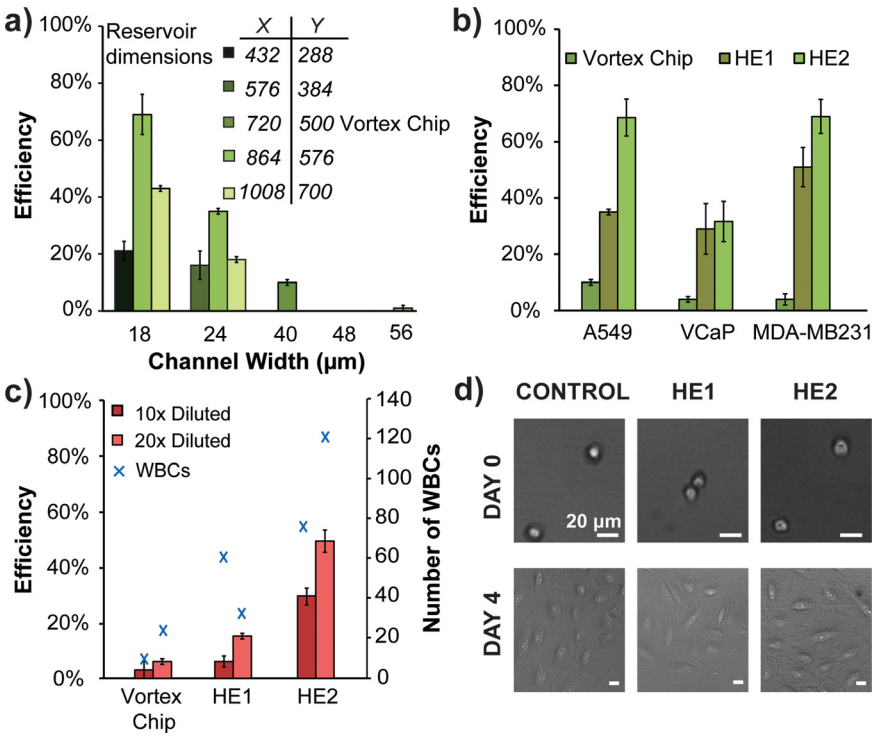


FIG. 3. Vortex HE provides higher efficiency capture for cancer cell lines. (a) Comparison of A549 capture efficiency of devices with different entry channel widths and reservoir sizes (N = 3). (b) Vortex HE devices are able to capture cancer cells at higher efficiencies than Vortex Chip (N = 3). (c) A549 cells were spiked in diluted whole blood. HE devices outperform the Vortex Chip for both 10× and 20× dilutions of blood (N = 3). (d) A549 cells are able to proliferate well after being processed through the HE devices.

18 $\mu$m, $U$ is increased from 3 m/s to 6 m/s; we can assume $f_L$ is approximately equal in both cases. Thus lift force increases by a factor of 9 from the Vortex Chip to HE2 and by a factor of 4.6 from Vortex Chip to HE1. The higher lift force helps particles cross the main streamline and increases their probability of entering the reservoirs. Further reducing the channel cross sectional area could potentially yield better results; however, higher pressure and device clogging would introduce operational issues.

In addition to the entry channel, the reservoir size also plays a role in capture efficiency. We find that scaling reservoir size down with channel widths of 18 $\mu$m or 24 $\mu$m only incrementally increases capture efficiency (Fig. S1).[29] However, a drastic improvement in capture occurs when we couple a narrow channel with a larger reservoir size of 864 × 576 $\mu$m (Fig. 3(a)). The increase in capture with the larger reservoirs may result from the higher volume capacity. A larger reservoir can hold the same or greater amount of particles as a smaller reservoir while reducing the probability of inter-particle interactions.

Further increasing the reservoir dimensions leads to less capture. We use a COMSOL simulation to show that the largest reservoir (700 × 1008 $\mu$m) has a greater part of the separatrix entering the reservoir than in slightly smaller reservoirs (Fig. S5).[29] Particles circulating in the reservoirs may have more opportunity along the separatrix boundary to leave the vortex trap because the separatrix region increases in length in the larger reservoirs. As the reservoir size increases, the parabolic shape of the main entry flow also readjusts leading to loss of lift-inducing curvature and reduces restoration force on a particle. These factors likely contribute to particles leaving reservoirs and a reduction in particle capture (Fig. 3(a)).

Consistent with entry and stability considerations, we find that Vortex HE effectively captures a broader size range of cancer cells from diluted whole blood. A549 cells were spiked in different dilutions of healthy blood and were processed through Vortex Chip, HE1, and HE2 devices. For all three devices, the capture efficiency was higher with 20× diluted blood

compared with 10× dilution, with up to 8 times better capture efficiency for device HE2 and 2.5 times better capture for device HE1. Though the number of WBCs captured by the new devices is higher than that by Vortex Chip, the purity of these devices remains comparable because the number of cancer cells captured concomitantly increases in the HE devices. In fact, the purity of the HE1 device is 66%, which is higher than the 46% purity seen in the Vortex Chip for 20× diluted blood. On average when using 20× diluted blood, the HE1 device and Vortex Chip capture comparable numbers of WBCs, and HE1 captures higher numbers of cancer cells.

### C. Cell proliferation assay

The Vortex HE device operates at a higher velocity and subsequently applies higher shear stress on the cancer cells. Such stress could negatively affect the cells. To assess this hypothesis, we investigated the viability and proliferation of the cells collected through the HE devices. Live/dead staining shows that cells processed through the HE1 and HE2 devices have a 96% ± 7% and 96% ± 3% (N = 3) viability, respectively, immediately after processing. Fig. 3(d) confirms that despite higher velocity and shear stress, cells collected with Vortex HE1 or HE2 were able to grow over 4 days. These confirm that higher velocity and shear stress do not affect viability or proliferation.

### D. CTC enrichment from clinical samples

The capability of the higher efficiency devices to capture CTCs was evaluated with blood samples from patients diagnosed with three common types of cancer. Blood samples from three NSCLC patients, three prostate cancer patients, and three breast cancer patients were processed (Supplementary Table 1),[29] as well as blood samples from healthy donors of the same age. We selected the Vortex HE1 device for capture of CTCs from cancer patient samples because the HE1 device is less prone to channel clogging than HE2 due to slightly larger channels and filter designs, making it usable for a longer processing time and larger blood sample volume. The same samples were also processed through the previous Vortex Chip for comparison. These samples were stained for CK, expressed in many cancer cells of epithelial origin, CD45 to identify WBCs, and DAPI to stain nuclei.

All three lung, all three prostate, and two of three breast cancer samples had higher numbers of CTCs captured with the Vortex HE1 device than with the Vortex Chip (Fig. 4(a)). When compared with the Vortex Chip device, the HE1 device captured on average 4 fold more total cells from cancer patients. A few cells that fit the criterion for CTCs were also seen in healthy samples, which can be used as a baseline threshold for disease. For healthy samples, the HE1 device captured, on average, two fold more cells than the Vortex Chip. Therefore, separate healthy thresholds have to be defined for each device. The maximum number of cells defined as CTCs found in the healthy samples was used as the threshold for each device. The threshold for Vortex HE and Vortex Chip is 1.5 CTCs/ml and 0.33 CTCs/ml, respectively. Both devices identified CTCs above threshold in 67% of the cancer patients. A size distribution of the CTCs collected shows that 60% of the CTCs Vortex HE1 collects are below 15 $\mu$m, whereas 30% of the CTCs captured by Vortex Chip are in this range (Fig. S5).[29] Capturing additional cells can aid in downstream molecular analysis and in sampling a larger section of tumor heterogeneity.

Interestingly, the HE1 device was able to capture rare CD45+ cells larger than normal WBCs for one breast cancer and one prostate cancer patient. These cells, which were not seen in our previous studies using the Vortex Chip, were larger than 20 $\mu$m, and showed a low nuclear to cytoplasm ratio (Fig. 4(b)). These cells could potentially be rare circulating macrophages, which has been observed by others as well.[34] The HE1 device may be capturing a rare population of WBCs that circulate in the blood stream in specific patients and conditions. Further investigations could potentially reveal new metrics for assessing disease states based on the number of rare large circulating cells beyond CTCs, which are effectively isolated with the new design.

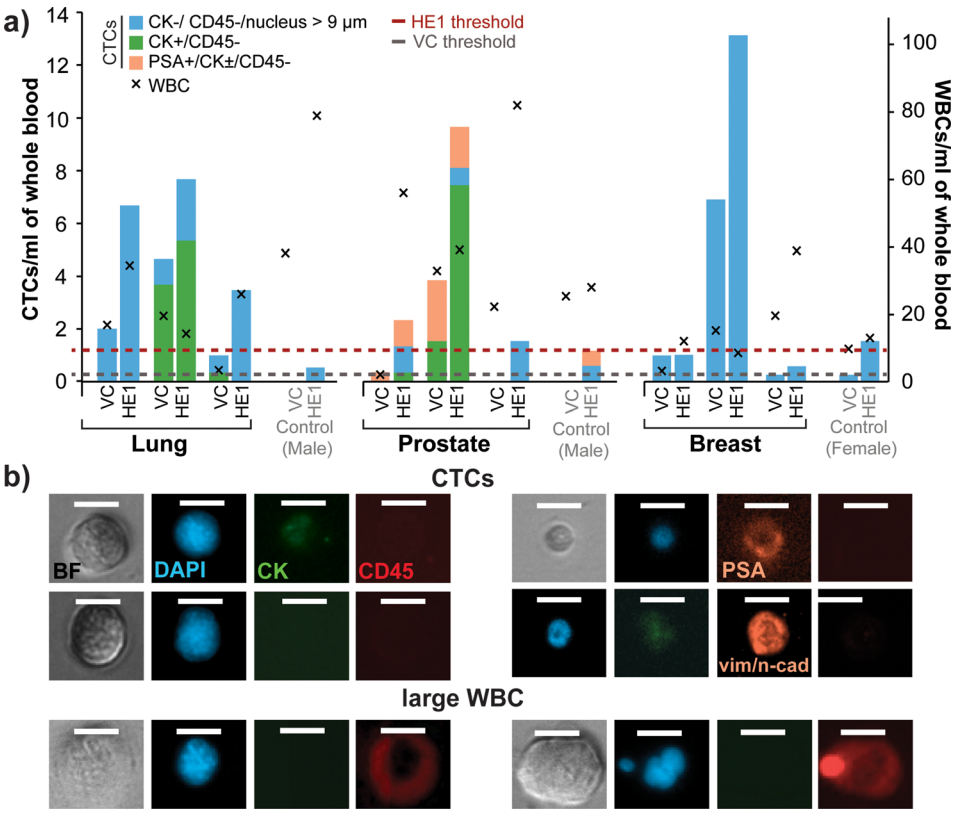


FIG. 4. Vortex HE provides improved capture performance for cancer patient samples. (a) Three blood samples each from lung, prostate, and breast cancer patients were collected and processed to compare the performance of Vortex Chip and HE1 devices. The HE1 device is able to collect more CTCs than Vortex Chip. Age-matched samples from two male and one female donors were used to set baseline thresholds. (b) Example of CTCs found from lung, breast, and prostate cancer patients (rows 1, 2, and 3, respectively). The 4th row shows a lung CTC expressing EMT markers. The 5th row shows an example of a rare large CD45+ cell that was collected and counted as WBC.

We also found a subset of CTCs from all three cancer types that lacked cytokeratin expression (DAPI+, CD45−, and large N/C ratio). To further characterize these CTCs, we investigated whether these cells possessed markers consistent with an EMT. Using a vimentin/N-Cadherin cocktail, immunostaining revealed that one lung and one breast cancer patient each had one cell that was negative for CK and positive for vimentin and/or N-Cadherin. One lung cancer sample also contained 7 cells that were positive for both vimentin/N-Cadherin and CK (Fig. S7).[29] Only cells collected from Vortex HE had EMT markers. These results indicate that Vortex HE is able to capture some rare CTCs that have transitioned to a mesenchymal state.

## V. CONCLUSIONS

We demonstrate that cell size cut-off in vortex-mediated rare cell trapping can be effectively controlled through the entry channel dimensions. The ability to tune particle size cut-off allows development of Vortex Chips for specific applications. Highest capture efficiency can be achieved using devices with the narrowest entry channel dimensions; however, sample purity and ease of processing are reduced. As such, this device may be most ideal for isolating cancer cells from dilute solutions such as pleural fluids. Intermediate entry channel dimensions (Vortex HE1 Chip) enable capture of a broader size range of CTCs while maintaining the higher purity of previous devices. Capturing a larger distribution of the CTC population along with high purity should enable a deeper look into the genomic landscape of CTCs as they relate to primary and metastatic tumors. Ultimately, these devices could be used to prepare liquid biopsies for a range of applications: to better personalize drugs to the patient's mutational or phenotypic

landscape as well as monitoring of therapeutic efficacy and development of resistance mutations or phenotypes.

## ACKNOWLEDGMENTS

The authors thank Dr. Oladunni Adeyiga, clinical coordinators, nurses, and all donors for their contributions toward blood sample collection. We thank Edward Pao for the PSA staining and Clementine Lemaire for the Vimentin/N-Cadherin staining optimization. This work was funded by Vortex Biosciences, Inc., and Office of Naval Research Young Investigator Program (Grant No. N000141210847). We would like to disclose the following conflicts of interest: The University of California, Los Angeles, D. Di Carlo, E. Sollier, and C. Renier have financial interests in Vortex Biosciences.

[1]H. W. Hou, M. E. Warkiani, B. L. Khoo, Z. R. Li, R. a Soo, D. S.-W. Tan, W.-T. Lim, J. Han, A. A. S. Bhagat, and C. T. Lim, Sci. Rep. **3**, 1259 (2013).
[2]M. Hosokawa, H. Kenmotsu, Y. Koh, T. Yoshino, T. Yoshikawa, T. Naito, T. Takahashi, H. Murakami, Y. Nakamura, A. Tsuya, T. Shukuya, A. Ono, H. Akamatsu, R. Watanabe, S. Ono, K. Mori, H. Kanbara, K. Yamaguchi, T. Tanaka, T. Matsunaga, and N. Yamamoto, PLoS One **8**, e67466 (2013).
[3]E. Ozkumur, A. M. Shah, J. C. Ciciliano, B. L. Emmink, D. T. Miyamoto, E. Brachtel, M. Yu, P. Chen, B. Morgan, J. Trautwein, A. Kimura, S. Sengupta, S. L. Stott, N. M. Karabacak, T. A. Barber, J. R. Walsh, K. Smith, P. S. Spuhler, J. P. Sullivan, R. J. Lee, D. T. Ting, X. Luo, A. T. Shaw, A. Bardia, L. V. Sequist, D. N. Louis, S. Maheswaran, R. Kapur, D. A. Haber, and M. Toner, Sci. Transl. Med. **5**, 179ra47 (2013).
[4]Y. Chen, P. Li, P.-H. Huang, Y. Xie, J. D. Mai, L. Wang, N.-T. Nguyen, and T. J. Huang, Lab Chip **14**, 626 (2014).
[5]S. Riethdorf, H. Fritsche, V. Müller, T. Rau, C. Schindlbeck, B. Rack, W. Janni, C. Coith, K. Beck, F. Jänicke, S. Jackson, T. Gornet, M. Cristofanilli, K. Pantel, V. Muller, C. Schindibeck, and F. Janicke, Clin. Cancer Res. **13**, 920 (2007).
[6]E. Andreopoulou, L. Y. Yang, K. M. Rangel, J. M. Reuben, L. Hsu, S. Krishnamurthy, V. Valero, H. A. Fritsche, and M. Cristofanilli, Int. J. Cancer **130**, 1590 (2012).
[7]A. Alva, T. Friedlander, M. Clark, T. Huebner, S. Daignault, M. Hussain, C. Lee, K. Hafez, B. Hollenbeck, A. Weizer, G. Premasekharan, T. Tran, C. Fu, C. Ionescu-Zanetti, M. Schwartz, A. Fan, and P. Paris, J. Urol. **194**, 790 (2015).
[8]B. P. Casavant, R. Mosher, J. W. Warrick, L. J. Maccoux, S. M. F. Berry, J. T. Becker, V. Chen, J. M. Lang, D. G. McNeel, and D. J. Beebe, Methods **64**, 137 (2013).
[9]S. L. Stott, C.-H. Hsu, D. I. Tsukrov, M. Yu, D. T. Miyamoto, B. A. Waltman, S. M. Rothenberg, A. M. Shah, M. E. Smas, G. K. Korir, F. P. Floyd, A. J. Gilman, J. B. Lord, D. Winokur, S. Springer, D. Irimia, S. Nagrath, L. V. Sequist, R. J. Lee, K. J. Isselbacher, S. Maheswaran, D. A. Haber, and M. Toner, Proc. Natl. Acad. Sci. U.S.A. **107**, 18392 (2010).
[10]N. Shao, E. Wickstrom, and B. Panchapakesan, Nanotechnology **19**, 465101 (2008).
[11]S. Wang, K. Liu, J. Liu, Z. T. F. Yu, X. Xu, L. Zhao, T. Lee, E. K. Lee, J. Reiss, Y. K. Lee, L. W. K. Chung, J. Huang, M. Rettig, D. Seligson, K. N. Duraiswamy, C. K. F. Shen, and H. R. Tseng, Angew. Chem.—Int. Ed. **50**, 3084 (2011).
[12]T. M. Gorges, I. Tinhofer, M. Drosch, L. Roese, T. M. Zollner, T. Krahn, and O. von Ahsen, BMC Cancer **12**, 178 (2012).
[13]L. Bai, Y. Du, J. Peng, Y. Liu, Y. Wang, Y. Yang, and C. Wang, J. Mater. Chem. B **2**, 4080 (2014).
[14]P. Li, Z. Mao, Z. Peng, L. Zhou, Y. Chen, P. Huang, and C. I. Truica, Proc. Natl. Acad. Sci. U.S.A. **112**, 4970 (2015).
[15]S. Zheng, H. Lin, J. Q. Liu, M. Balic, R. Datar, R. J. Cote, and Y. C. Tai, J. Chromatogr. A **1162**, 154 (2007).
[16]P. R. C. Gascoyne and S. Shim, Cancers (Basel) **6**, 545 (2014).
[17]G. Vona, A. Sabile, M. Louha, V. Sitruk, S. Romana, D. Franco, M. Pazzagli, M. Vekemans, B. Lacour, and P. Paterlinibre, Am. J. Pathol. **156**, 57 (2000).
[18]X. Qin, S. Park, S. P. Duffy, K. Matthews, R. R. Ang, T. Todenhöfer, H. Abdi, A. Azad, J. Bazov, K. N. Chi, P. C. Black, and H. Ma, Lab Chip **15**, 2278 (2015).
[19]A. A. S. Bhagat, H. W. Hou, L. D. Li, C. T. Lim, and J. Han, Lab Chip **11**, 1870 (2011).
[20]S. C. Hur, N. K. Henderson-MacLennan, E. R. B. McCabe, and D. Di Carlo, Lab Chip **11**, 912 (2011).
[21]H. Amini, W. Lee, and D. Di Carlo, Lab Chip **14**, 2739 (2014).
[22]E. Sollier, D. E. Go, J. Che, D. R. Gossett, S. O. Byrne, M. Weaver, N. Kummer, M. Rettig, J. Goldman, N. Nickols, S. O'Byrne, W. M. Weaver, N. Kummer, M. Rettig, J. Goldman, N. Nickols, S. McCloskey, R. P. Kulkarni, and D. Di Carlo, Lab Chip **14**, 63 (2014).
[23]S. C. Hur, A. J. Mach, and D. Di Carlo, Biomicrofluidics **5**, 022206 (2011).
[24]A. J. Mach, J. H. Kim, A. Arshi, S. C. Hur, and D. Di Carlo, Lab Chip **11**, 2827 (2011).
[25]M. Gerlinger, A. J. Rowan, S. Horswell, J. Larkin, D. Endesfelder, E. Gronroos, P. Martinez, N. Matthews, A. Stewart, P. Tarpey, I. Varela, B. Phillimore, S. Begum, N. Q. McDonald, A. Butler, D. Jones, K. Raine, C. Latimer, C. R. Santos, M. Nohadani, A. C. Eklund, B. Spencer-Dene, G. Clark, L. Pickering, G. Stamp, M. Gore, Z. Szallasi, J. Downward, P. A. Futreal, and C. Swanton, N. Engl. J. Med. **366**, 883 (2012).
[26]H. Bai, Z. Wang, Y. Wang, M. Zhuo, Q. Zhou, J. Duan, L. Yang, M. Wu, T. An, J. Zhao, and J. Wang, PLoS One **8**, e54170 (2013).
[27]Z.-Y. Chen, W.-Z. Zhong, X.-C. Zhang, J. Su, X.-N. Yang, Z.-H. Chen, J.-J. Yang, Q. Zhou, H.-H. Yan, S.-J. An, H.-J. Chen, B.-Y. Jiang, T. S. Mok, and Y.-L. Wu, Oncologist **17**, 978 (2012).

[28]L. G. Martelotto, C. K. Ng, S. Piscuoglio, B. Weigelt, and J. S. Reis-Filho, Breast Cancer Res. **16**, R48 (2014).
[29]See supplementary material at http://dx.doi.org/10.1063/1.4937895 for additional data.
[30]J. Friend and L. Yeo, Biomicrofluidics **4**, 26502 (2010).
[31]I. F. Sbalzarini and P. Koumoutsakos, J. Struct. Biol. **151**, 182 (2005).
[32]J. Che, V. Yu, M. Dhar, C. Rennier, M. Matsumoto, K. Heirich, E. B. Garon, Edward, J. Goldman, J. Rao, S. S. Jeffrey, R. P. Kulkarni, E. Sollier, and D. Di Carlo, "Classification of large circulating tumor cells isolated with ultra-high throughput microfluidic Vortex technology," Cancer Res. (submitted).
[33]R. D. Jiang, H. Shen, and Y. J. Piao, Rom. J. Morphol. Embryol. **51**, 663 (2010).
[34]D. L. Adams, S. S. Martin, R. K. Alpaugh, M. Charpentier, S. Tsai, R. C. Bergan, I. M. Ogden, W. Catalona, S. Chumsri, C.-M. Tang, and M. Cristofanilli, Proc. Natl. Acad. Sci. U.S.A. **111**, 3514 (2014).